Scale-dependent bias of galaxies and μ-type distortion of the cosmic microwave background spectrum from single-field inflation with a modified initial state

Jonathan Ganc
Texas Cosmology Center and the Department of Physics, The University of Texas at Austin, 1 University Station, C1600, Austin, TX 78712

Eiichiro Komatsu
Texas Cosmology Center and the Department of Astronomy, The University of Texas at Austin, 1 University Station, C1400, Austin, TX 78712
Kavli Institute for the Physics and Mathematics of the Universe, Todai Institutes for Advanced Study, the University of Tokyo, Kashiwa, Japan 277-8583 (Kavli IPMU, WPI) and
Max Planck Institut für Astrophysik, Karl-Schwarzschild-Str. 1, 85741 Garching, Germany

We investigate the phenomenological consequences of a modification of the initial state of quantum fluctuations of a single inflationary field. While single-field inflation with the standard Bunch-Davies initial vacuum state does not generally produce a measurable three-point function (bispectrum) in the so-called squeezed triangle configuration (where one wavenumber, k, is much smaller than the other two, $k \ll k_1 \approx k_2$), allowing for a non-standard initial state produces an exception. Here, we calculate the signature of an initial state modification in single-field slow-roll inflation as it would appear in both the scale-dependent bias of the large-scale structure (LSS) and μ-type distortion in the black-body spectrum of the cosmic microwave background (CMB). We parametrize the initial state modifications and identify certain choices of parameters as natural, though we also note some fine-tuned choices that can yield a larger bispectrum. In both cases, we observe a distinctive k^{-3} signature in LSS (as opposed to the k^{-2} of the so-called local-form bispectrum). As a non-zero bispectrum in the squeezed configuration correlates one long-wavelength mode with two short-wavelength modes, it induces a correlation between the CMB temperature anisotropy observed on large scales with the temperature-anisotropy-squared on very small scales; this correlation persists as the small-scale anisotropy-squared is processed into the μ-type distortion of the black-body spectrum. While the correlation induced by the local-form bispectrum turns out to be too small to detect in near future, a modified initial vacuum state enhances the signal by a large factor owing to an extra factor of k_1/k compared to the local form. For example, a proposed absolutely-calibrated experiment, PIXIE, is expected to detect this correlation with a signal-to-noise ratio greater than 10, for an occupation number of about 0.5 in the observable modes. Relatively-calibrated experiments such as Planck and LiteBIRD should also be able to measure this effect, provided that the relative calibration between different frequencies meets the required precision. Our study suggests that the CMB anisotropy, the distortion of the CMB black-body spectrum, and the large-scale structure of the universe offer new ways to probe the initial state of quantum fluctuations.

I. INTRODUCTION

While cosmologists have accumulated extensive evidence for an early-universe inflationary period, the cause and dynamical specifics of that epoch remain unclear. Current and upcoming measurements will provide increasingly precise measurements of the effects of inflation, demanding that theorists persist in relating these observations to inflation's underlying mechanism. Primordial non-Gaussianity is a popular discriminant among the proposed models of inflation (e.g., [1–3]).

The scalar curvature perturbation, ζ, which appears in the space-space part of the metric in a suitable gauge as $g_{ij} = a^2(t)e^{2\zeta}\delta_{ij}$ (where $a(t)$ is the Robertson-Walker scale factor), is a convenient quantity relating the observables such as the cosmic microwave background (CMB) and the large-scale structure (LSS) of the universe to the primordial perturbations generated during inflation. In particular, this quantity is conserved outside the horizon for single-field inflation (e.g., [4]). We shall define the two-point function (power spectrum, denoted as $P_\zeta(k)$) and the three-point function (bispectrum, denoted as $B_\zeta(k_1, k_2, k)$) of ζ in Fourier space as follows:

$$\langle \zeta_{\mathbf{k}_1} \zeta_{\mathbf{k}} \rangle = (2\pi)^3 \delta(\mathbf{k}_1 + \mathbf{k}) P_\zeta(k), \quad (1)$$

$$\langle \zeta_{\mathbf{k}_1} \zeta_{\mathbf{k}_2} \zeta_{\mathbf{k}} \rangle = (2\pi)^3 \delta(\mathbf{k}_1 + \mathbf{k}_2 + \mathbf{k}) B_\zeta(k_1, k_2, k). \quad (2)$$

The current data constrain the shape of $P_\zeta(k)$ as $P_\zeta(k) \propto k^{n_s - 4}$ with $n_s = 0.96 \pm 0.01$ [5, 6].

The so-called local-form bispectrum defined as [7, 8]

$$B_\zeta^{\rm local}(k_1, k_2, k) \equiv \frac{6}{5} f_{\rm NL} \left[P_\zeta(k_1) P_\zeta(k_2) + (2 \text{ perm.}) \right], \quad (3)$$

is particularly interesting, both because a detection of the primordial bispectrum at the level of $f_{\rm NL} \gg 1$ would disfavor single-field inflation [9–12] and because it is easy to measure the primordial signal since few late-time effects can produce the local-form bispectrum. The most important contamination of $f_{\rm NL}$ known to date is due to the lensing-Integrated Sachs-Wolfe (ISW) effect bispectrum

[13], which can be calculated precisely and removed. The contamination of $f_{\rm NL}$ due to non-linearity in the photon-baryon fluid has been shown to be at most one [14].

The local-form bispectrum has the largest signal in the so-called "squeezed triangle configuration," for which one of the wavenumbers, say, k, is much smaller than the other two, $k \ll k_1 \approx k_2$. This can be seen from Eq. (3): as $P_\zeta(k) \propto k^{-3}$ for a scale-invariant spectrum ($n_s = 1$), the bispectrum is maximized when k is taken to be small. In this limit, one finds:

$$B^{\rm local}(k_1, k_1, k \to 0) \to \frac{12}{5} f_{\rm NL} P_\zeta(k_1) P_\zeta(k) \propto \frac{1}{k_1^3 k^3}, \quad (4)$$

for a scale-invariant spectrum.

Recently, Agullo and Parker have shown that a non-standard initial state of quantum fluctuations generated during single-field inflation can enhance the bispectrum in the squeezed configuration by a factor of k_1/k, i.e., $B(k_1, k_1, k \to 0) \propto 1/(k_1^2 k^4)$ [15]. This would have profound implications for observations of the bispectrum in the squeezed configuration. For example, the signature in the bispectrum of CMB of this model was investigated in a paper by one of the authors [16], who found that the model could produce a measurable local $f_{\rm NL}$ signal in the CMB.

The primordial bispectrum in the squeezed configuration was initially constrained mostly by measurements of the temperature anisotropy of the CMB [5, 17]. However, over time, tools for observing the bispectrum have proliferated, providing a variety of ways to compare inflationary models. In this paper, we will explore two such methods:

1. In the large scale-structure (LSS) of the universe, the local-form bispectrum leaves a signature by contributing a scale-dependence to the halo bias, $b(k)$ [18–20]. For the local-form bispectrum, the scale dependence goes as $1/k^2$; however, for a modified initial state, this scale dependence can become $1/k^3$.

2. Anisotropy in the so-called μ-type distortions of the black-body spectrum of the CMB can be correlated with the CMB temperature anisotropy measured on large scales. This correlation can be used to measure the bispectrum in the squeezed configuration but with a larger value of k_1/k than previously thought possible [21].

This paper is organized as follows. In Section II, we review the model under consideration. In Section III, we give the form of the bispectrum and comment on potential uncertainties in the results. In Section IV, we discuss a useful approximation to the bispectrum in the squeezed configuration. In Section V, we calculate the signal of this model in the scale-dependent bias of LSS. In Section VI, we calculate the signal of this model in the μ-type distortion of the CMB black-body spectrum, correlated with the CMB temperature anisotropy on large scales. Finally, we conclude in Section VII.

Throughout this paper, we shall set $M_{\rm pl} \equiv 1/\sqrt{8\pi G} \equiv 1$, and use the cosmological parameters given by the WMAP 5-year best-fit parameters (WMAP+BAO+H_0 ML; [22]): $\Omega_M = 0.277$, $\Omega_\Lambda = 0.723$, $h = 0.702$, $n_s = 0.962$, and $\Delta^2_\zeta(k_0 = 0.002\ {\rm Mpc}^{-1}) = 2.46 \times 10^{-9}$, unless stated otherwise.

II. ACTION AND MODE FUNCTION

We consider here single-field slow-roll inflation with a canonical kinetic term, where the action (to lowest order in slow-roll) can be written as [9]

$$\begin{aligned} S =& S_2 + S_3\,, \\ S_2 =& \frac{1}{2}\int d^4x \frac{\dot\phi^2}{H^2}[a^3\dot\zeta^2 - a(\partial\zeta)^2], \\ S_3 =& \int d^4x \frac{\dot\phi^4}{H^4} a^5 H \dot\zeta^2 \partial^{-2}\dot\zeta. \end{aligned} \quad (5)$$

We expand the curvature perturbation into creation, $a^\dagger_{\mathbf{k}}$, and annihilation, $a_{\mathbf{k}}$, operators (not to be confused with the Robertson-Walker scale factor, $a(t)$):

$$\zeta(\mathbf{x}, t) = \int \frac{d^3\mathbf{k}}{(2\pi)^3}\left[a_{\mathbf{k}} u_k(t) e^{i\mathbf{k}\cdot\mathbf{x}} + a^\dagger_{\mathbf{k}} u^*_k(t) e^{-i\mathbf{k}\cdot\mathbf{x}}\right]. \quad (6)$$

Usually, one chooses an initial state so that a comoving observer in the approximately de Sitter spacetime observes no particles (i.e., for this observer $a_{\mathbf{k}}|0\rangle = 0$). This implies a positive-frequency mode function given by

$$u_k(\eta) = \frac{H^2}{\dot\phi}\frac{1}{\sqrt{2k^3}}(1 + ik\eta)e^{-ik\eta}, \quad (7)$$

where $\eta \equiv \int^t \frac{dt'}{a(t')}$ is the conformal time; for future reference, we note

$$u'_k \equiv \frac{\partial u_k}{\partial \eta} = \frac{H^2}{\dot\phi}\sqrt{\frac{k}{2}}\eta e^{-ik\eta}. \quad (8)$$

While this is certainly a reasonable assumption, it is an assumption, and all assumptions must be tested by observations. Thus, a responsible scientist should ask: *"If the initial state of ζ was not in this preferred vacuum state (known as the Bunch-Davies state), what are the implications for observations?"* Our goal in this paper is not to construct candidate models of a modified initial state, but to study phenomenological consequences of such a modification, i.e., to let our observations tell us about the initial state of quantum fluctuations.

Once we adopt this approach, the next question is: "How should we parametrize a modified initial state?" We will represent a modified initial state as a Bogoliubov transformation of the above Bunch-Davies mode function:

$$\tilde u_k(\eta) = \alpha_k u_k(\eta) + \beta_k u^*_k(\eta). \quad (9)$$

This is not the most general form one can write down (see, e.g., [23]), but it provides us with a reasonable starting point. In line with our previous goal, we will take the Bogoliubov coefficients as given rather than trying to derive them from a fundamental theory. From the commutation relation of creation and annihilation operators, the coefficients α_k and β_k must satisfy $|\alpha_k|^2 - |\beta_k|^2 = 1$. We also find that the occupation number of particles N_k, i.e., the expected number density of particles with momentum k, is given by $|\beta_k|^2$.

These Bogoliubov coefficients, α_k and β_k, encode information about physics on scales where we have limited information; thus, they can vary widely without inconsistency. However, we can place some constraints on the coefficients by demanding that the theory reproduce the observed power spectrum (including the spectral tilt, $n_s = 0.96 \pm 0.01$) and that the energy in the fluctuations not back-react on the background inflaton dynamics [23–25]. These requirements can be satisfied in a fairly natural way if we suppose that the coefficients are such that $\langle N_k \rangle \approx N_{k,0} e^{-k^2/k_{\rm cut}^2}$, where the cutoff momentum $k_{\rm cut}$ must be specified. The values allowed for $N_{k,0}$ depend on the value of $k_{\rm cut}$ [25]; for $k_{\rm cut} \approx \sqrt{M_{\rm pl} H}$, i.e., the scale of inflation, $N_{k,0}$ can be of order unity. Additionally, if we suppose that the smallest primordial scales observable today come from momenta sufficiently smaller than $k_{\rm cut}$, then $\langle N_k \rangle \approx N_{k,0} \equiv N$, i.e., roughly constant in k. Remembering that $\langle N_k \rangle = |\beta_k|^2$ and that only the relative phase between α_k and β_k is significant, we parametrize

$$\alpha_k \equiv \sqrt{1+N} e^{i\theta_k}, \qquad \beta_k \equiv \sqrt{N}\,. \tag{10}$$

There is still uncertainty with respect to θ_k. As explained further in [16], we identify two scenarios as plausible behaviors: 1) $\theta_k \approx k\eta_0$, where $k|\eta_0| \gg 1$ for relevant k, and 2) $\theta_k \approx {\rm const} \equiv \theta$. In the latter scenario, one can tune the value of θ to give larger effects; we will generally show results that assume the value of θ that gives the largest signal. In this sense (and for another reason discussed in [16]), we consider the former scenario to be more conservative.

III. POWER SPECTRUM AND BISPECTRUM

The power spectrum of ζ on super-horizon scales, $k\eta \ll 1$, which seeds the observed fluctuations, is given simply by $P_\zeta(k) = |\tilde{u}_k(\eta \to 0)|^2$ [16], i.e.,

$$P_\zeta(k) = \frac{H^4}{\dot\phi^2} \frac{1}{2k^3} \left|\alpha_k + \beta_k\right|^2, \tag{11}$$

which becomes (using Eq. (10))

$$P_\zeta(k) = \frac{H^4}{\dot\phi^2} \frac{1}{2k^3} \left(1 + 2N + 2\sqrt{N(N+1)}\cos\theta_k\right). \tag{12}$$

The calculation of the bispectrum requires more thought. Formally, it is given by [9]

$$\begin{aligned} &\langle \zeta_{\mathbf{k}_1}(t)\zeta_{\mathbf{k}_2}(t)\zeta_{\mathbf{k}}(t)\rangle \\ &= -i\int_{t_0}^{t} dt' \langle [\zeta_{\mathbf{k}_1}(t)\zeta_{\mathbf{k}_2}(t)\zeta_{\mathbf{k}}(t), H_{\rm int}(t')]\rangle, \end{aligned} \tag{13}$$

where the interaction Hamiltonian, $H_{\rm int}$, is given by $\int dt' H_{\rm int}(t') = -S_3$ with S_3 given by Eq. (5). We would then specify the initial state at the initial time, t_0, or equivalently at the initial conformal time, η_0. For the action given by Eq. (5), one finds

$$\begin{aligned} B_\zeta(k_1,k_2,k) = 2i\frac{\dot\phi^4}{H^6} \frac{k_1^2k_2^2 + k_2^2k^2 + k^2k_1^2}{k_1^2k_2^2k^2} \tilde{u}_{k_1}\tilde{u}_{k_2}\tilde{u}_k \\ \times \int_{\eta_0}^{\eta} \frac{d\eta'}{(\eta')^3} \tilde{u}'^*_{k_1}\tilde{u}'^*_{k_2}\tilde{u}'^*_k + \text{c. c. }. \end{aligned} \tag{14}$$

In this paper, dots will denote derivatives with respect to t and primes will denote derivatives with respect to η. For the standard calculation, we take the Bunch-Davies initial vacuum state, given by $\alpha_k = 1$ and $\beta_k = 0$, for all modes into the infinite past, $\eta_0 \to -\infty$ (i.e., $t \to 0$). For this case, there is an accepted prescription for calculations: we take $\eta_0 \to \eta_0 + i\epsilon|\eta_0|$, giving η an imaginary component when its absolute value is large [9]. The exponential terms in the integrand like $e^{i(k_1+k_2+k)\eta_0}$ (see (8) for their origin) would ordinarily oscillate rapidly at very early times but are suppressed by the imaginary part of η_0. Note that this suppression depends on $k_1+k_2+k > 0$.

However, when we allow for a more general initial state, we can have $\beta_k \neq 0$ resulting in terms like $e^{i(-k_1+k_2+k)\eta_0}$, $e^{i(-k_1-k_2+k)\eta_0}$, etc. Furthermore, one may object (e.g., for reasons of renormalizability) to setting initial conditions in the infinite past, especially if some of the modes are excited (i.e., $\beta_k \neq 0$); instead, one might prefer that initial conditions be set at some finite time. If we ignore this objection for a moment, one can still suppose that $\eta_0 \to \eta_0 + i\epsilon|\eta_0|$. By triangle inequalities (e.g., $k_1 \leq k_2 + k$, etc.), the exponentials are still suppressed except at the precise folded limit $k_1 = k_2 + k$ (note that this would result in Eq. (15) but without the exponentials).

In this paper, however, we will generally take the objection seriously and suppose that initial conditions were not set infinitely far in the past. Unfortunately, this draws us into an area of active research which does not offer a definite formalism for calculations. Here, as in [26] (though see [27, 28]), we will adopt the "Boundary Effective Field Theory" approach to non-Bunch Davies initial conditions [29], which like the other available approaches is not without problems (e.g., [30]). In this approach, one cuts off the integral given in Eq. (13) at a finite η_0, where the initial conditions are set.

We shall assume that for excited modes k (i.e., where $\beta_k \neq 0$), $k|\eta_0| \gg 1$ so that k was deep inside the horizon at the initial time. This can be explained as expressing the requirement that the process for mode excitation was causal and thus, could only excite subhorizon modes.

Performing the integral given in Eq. (14), one obtains the bispectrum [16]

$$B_\zeta(k_1,k_2,k) = \frac{1}{2}\frac{H^6}{\dot\phi^2}\frac{k_1^2k_2^2+k_2^2k^2+k^2k_1^2}{k_1^3k_2^3k^3} \times \Re\Big[\frac{1}{k_1+k_2+k}F_{\alpha\alpha\alpha}\left(1-e^{i(k_1+k_2+k)\eta_0}\right) + \frac{1}{k_1+k_2-k}F_{\alpha\alpha\beta}\left(1-e^{i(k_1+k_2-k)\eta_0}\right) + \frac{1}{k_1-k_2+k}F_{\alpha\beta\alpha}\left(1-e^{i(k_1-k_2+k)\eta_0}\right) + \frac{1}{-k_1+k_2+k}F_{\beta\alpha\alpha}\left(1-e^{i(-k_1+k_2+k)\eta_0}\right)\Big], \quad (15)$$

where

$$F_{XYZ} \equiv (\alpha_{k_1}+\beta_{k_1})(\alpha_{k_2}+\beta_{k_2})(\alpha_k+\beta_k)X^*_{k_1}Y^*_{k_2}Z^*_k - (\alpha^*_{k_1}+\beta^*_{k_1})(\alpha^*_{k_2}+\beta^*_{k_2})(\alpha^*_k+\beta^*_k)X^{\rm C}_{k_1}Y^{\rm C}_{k_2}Z^{\rm C}_k, \quad (16)$$

for $\alpha^{\rm C}\equiv\beta$, $\beta^{\rm C}\equiv\alpha$; F_{XYZ} gives information about the initial conditions at η_0. Note that we ignore a field redefinition term (derived in [9]) that is negligibly small for the purposes of this paper.

First, note that we recover the standard Bunch-Davies result [9] if we set $F_{\alpha\alpha\alpha}=1$, $F_{\alpha\alpha\beta}=F_{\alpha\beta\alpha}=F_{\beta\alpha\alpha}=0$, and $\eta_0\to-(1-i\epsilon)\infty$. In the squeezed limit, $k\ll k_1\approx k_2$ and we get $B_\zeta\to 2\frac{\dot\phi^2}{2H^2}P_\zeta(k_1)P_\zeta(k)$, where $\frac{\dot\phi^2}{2H^2}\approx 10^{-2}$ is the slow-roll parameter, which is equivalent to $f_{\rm NL}=\mathcal{O}(10^{-2})$ (see Eq. (4)). If we restore the field-redefinition piece we ignored, we obtain the full standard squeezed-limit bispectrum: $B_\zeta\to(1-n_s)P_\zeta(k_1)P_\zeta(k)$ [9].

Since we have assumed $k|\eta_0|\gg 1$, the exponentials in the bispectrum (15) oscillate rapidly and can, to a decent approximation, be ignored. Then, one sees that the bispectrum peaks in the so-called "folded triangle configuration," where one of the wavenumbers is approximately equal to the sum of the other two, i.e., $k\approx k_1+k_2$, $k_2\approx k_1+k$, or $k_1\approx k_2+k$; this was noted earlier by [26, 27, 31]. Since the local bispectrum has no corresponding peak, this regime provides a way to distinguish the shape of this bispectrum from a purely local form. We shall come back to this point in Section VII.

We can also investigate the squeezed configuration $k\ll k_1\approx k_2$; this configuration is in fact a special case of the folded limit $k_1\approx k_2+k$ when we additionally suppose that k is much smaller than k_1 or k_2. In this limit, the third and fourth terms are larger than the first and second by a factor of $k_1/k\gg 1$; the bispectrum becomes $B_\zeta\propto 8\frac{\dot\phi^2}{2H^2}\frac{k_1}{k}P_\zeta(k_1)P_\zeta(k)$ (with a proportionality factor $|\alpha_{k_1}+\beta_{k_1}|^{-2}|\alpha_k+\beta_k|^{-2}\Re\left[F_{\alpha\beta\alpha}(1-e^{ik\eta_0})\right]$). Note that this is enhanced relative to the local form in the squeezed configuration [15].

We should highight that the exponential terms cannot be completely ignored [27] because they prevent the bispectrum from blowing up in the folded limit. In particular, the factor $\frac{1}{-k_1+k_2+k}[1-e^{i(-k_1+k_2+k)\eta_0}]$, which seems to blow up in the folded limit if one ignores the exponential, actually goes as $-i\eta_0+\mathcal{O}((-k_1+k_2+k)\eta_0^2)$. Accounting for this behavior plays a role in the usefullness of the approximation we demonstrate in the next section.

IV. APPROXIMATION TO THE BISPECTRUM IN THE SQUEEZED CONFIGURATION

While the full form of the bispectrum given by Eq. (15) is complicated, the observables that we shall discuss in this paper (the scale-dependent halo bias in LSS and the anisotropy in the μ-type distortion of the CMB blackbody spectrum) depend primarily on the squeezed configuration, $k\ll k_1\approx k_2$. Therefore, it is useful to find an accurate approximation to the bispectrum in the squeezed configuration.

In [16], the author expanded to the lowest order in k (k here is equal to k_3 in [16]) after averaging over the exponential. Specifically, he approximated

$$\frac{1-e^{i(k_1-k_2+k)\eta_0}}{k_1-k_2+k}\approx\frac{1}{k}\,. \quad (17)$$

This result is also consistent with a prescription of ignoring oscillating terms by taking $\eta_0\to\eta_0+i\epsilon|\eta_0|$ for large $|\eta_0|$, as discussed in the previous section.

When we do not ignore oscillating terms, the approximation demonstrates the correct scaling on large scales but it is off by a factor. This arises because the approximation does not properly account for the oscillatory behavior of Eq. (17) at small k.

Fortunately, we can come up with a better approximation. Observe that, when calculating observables, the bispectrum is usually multiplied by a function and then integrated over some of the wavenumbers (see, e.g., Eq. (32) below). Let us focus on the integral over k_2. Note that the limits of integration for k_2 are $k_2\in[|k_1-k|,k_1+k]$; in the squeezed limit, the function multiplying the bispectrum will vary little over this small range, while the oscillatory terms like the left hand side of Eq. (17) will vary very rapidly. Thus, we can perform the k_2 integral only over the rapidly oscillating term, e.g.,

$$\int dk_1\int_{k_1-k}^{k_1+k}dk_2\,\cdots\frac{1-e^{i(k_1-k_2+k)\eta_0}}{k_1-k_2+k}\approx \approx\int dk_1\,\cdots\Big|_{k_2=k_1}\left(\int_{k_1-k}^{k_1+k}dk_2\frac{1-e^{i(k_1-k_2+k)\eta_0}}{k_1-k_2+k}\right). \quad (18)$$

For this integral, we find

$$\int_{k_1-k}^{k_1+k}dk_2\frac{1-e^{i(k_1-k_2+k)\eta_0}}{k_1-k_2+k} = [\gamma-{\rm Ci}(-2k\eta_0)+\log(-2k\eta_0)]+i\,{\rm Si}(-2k\eta_0) \approx\gamma-{\rm Ci}(-2k\eta_0)+\log(-2k\eta_0)\,,$$

where $\gamma \approx 0.5772$ is Euler's constant, $\mathrm{Ci}(z) \equiv -\int_z^\infty dt\cos(t)/t$ is the cosine integral, and $\mathrm{Si}(z) \equiv \int_0^z dt\sin(t)/t$ is the sin integral (which is $\sim \pi/2$ for $z > 1$); in the last line, we have dropped the second term since it becomes increasingly unimportant for large $k\eta_0$.

If we perform this new approximation, we find that, for $\theta \approx k\eta_0$, the chief contributor to the squeezed bispectrum looks like

$$B_{\zeta,k\ll k_1}^{\theta_k\approx k\eta_0}(k_1,k_2,k) \approx \frac{H^6}{\dot\phi^2}\frac{1}{k_1k_2k^4} \times N(1+N) \times \frac{1}{2}[\gamma - \mathrm{Ci}(-2k\eta_0) + \log(-2k\eta_0)]. \tag{19}$$

For $\theta_k \approx \mathrm{const} \equiv \theta$, we find

$$B_{\zeta,k\ll k_1}^{\theta_k\approx \mathrm{const}}(k_1,k_2,k) \approx \frac{H^6}{\dot\phi^2}\frac{1}{k_1k_2k^4} \times \Big[N(1+N)(3-\cos 2\theta) + \sqrt{N(1+N)}(1+2N)\cos\theta\Big] \times \frac{1}{2}[\gamma - \mathrm{Ci}(-2k\eta_0) + \log(-2k\eta_0)]. \tag{20}$$

These two equations provide useful approximations to the bispectrum from a modified initial state in the squeezed configuration.

Note that we can also view this approximation as finding a sort of average for the left hand side of (17), i.e., that

$$\left[\frac{1-e^{i(k_1-k_2+k)\eta_0}}{k_1-k_2+k}\right]_{avg} \equiv \frac{1}{2k}\int_{k_1-k}^{k_1+k} dk_2 \frac{1-e^{i(k_1-k_2+k)\eta_0}}{k_1-k_2+k} \approx \frac{\gamma - \mathrm{Ci}(-2k\eta_0) + \log(-2k\eta_0)}{2k}.$$

Thus, ignoring the oscillating terms in the bispectrum (as in [16]) is equivalent to neglecting a factor $\frac{1}{2}[\gamma - \mathrm{Ci}(-2k\eta_0) + \log(-2k\eta_0)]$, so that the regime investigated in [16] differs from the one here by a factor of order unity.

V. SCALE-DEPENDENT BIAS

How can we measure $B_\zeta(k_1,k_2,k)$ observationally? Obvious observables are the bispectrum of the CMB temperature and polarization anisotropy, and that of the matter density distribution in LSS. These observables are (in linear theory) related to $B_\zeta(k_1,k_2,k)$ in a straightforward way [8, 32].

A much less obvious observable is the *power spectrum* of dark matter halos (in which galaxies and clusters of galaxies would be formed). Dark matter halos are formed only at the locations of peaks of the underlying matter distribution. While the power spectrum of the underlying matter distribution is insensitive to the bispectrum, the power spectrum of *peaks* is sensitive to the bispectrum as well as to higher-order correlation functions [33]. This leads to a remarkable prediction: one can use the observed power spectrum of the distribution of galaxies (and of clusters of galaxies) to measure the bispectrum of primordial fluctuations [18–20].

In general, as the power spectrum of peaks (hence halos) is different from that of the underlying matter distribution, we say that halos are biased tracers of the underlying matter distribution [34]. The degree of bias is often parametrized by the so-called "bias factor," $b(k)$, defined as

$$b^2(k) \equiv \frac{P_{\rm halo}(k)}{P_{\rm matter}(k)}. \tag{21}$$

Alternatively, one may define $b(k)$ as the ratio of the matter-halo cross power spectrum to the matter power spectrum.

On large scales, where the matter density fluctuations are still in the linear regime, $b(k)$ approaches a constant for Gaussian matter density fluctuations, $b(k) \to b_1$. However, the presence of the primordial bispectrum leads to a non-trivial k-dependence in $b(k)$, and this is called a "scale-dependent bias."

Building on the previous work on the peak statistics [20, 33], Desjacques, Jeong, and Schmidt arrived at the following formula for $b(k)$ [35]:

$$\Delta b(k,R) = 2\frac{\mathcal{F}_R(k)}{\mathcal{M}_R(k)}\left[(b_1-1)\delta_c + \frac{d\ln\mathcal{F}_R(k)/d\ln R}{d\ln\sigma_R/d\ln R}\right], \tag{22}$$

where $\Delta b(k,R) \equiv b(k,R) - b_1$, $\delta_c = 1.686$, R is related to the mass of halos under consideration as $M = \frac{4\pi}{3}\Omega_M\rho_c R^3$, and $\rho_c = 2.775\times 10^{11}\ h^2\ M_\odot\ \mathrm{Mpc}^{-3}$ is the present-day critical density of the universe. The various functions are defined by

$$\mathcal{F}_R(k) \equiv \frac{1}{4\sigma_R^2 P_\zeta(k)}\int\frac{d^3k_1}{(2\pi)^3}\mathcal{M}_R(k_1)\mathcal{M}_R(|\mathbf{k}_1+\mathbf{k}|) \times B_\zeta(k_1,|\mathbf{k}_1+\mathbf{k}|,k), \tag{23}$$

$$\sigma_R^2 \equiv \int\frac{d^3k}{(2\pi)^3}P_\zeta(k)\mathcal{M}_R^2(k), \tag{24}$$

$$\mathcal{M}_R(k) \equiv \frac{2k^2D(z)}{5\Omega_M H_0^2}T(k)W_R(k)\,, \tag{25}$$

$$W_R(k) \equiv \frac{3j_1(kR)}{kR}, \tag{26}$$

$$\tag{27}$$

where $T(k)$ is the linear transfer function normalized such that $T(k)\to 1$ for $k\to 0$, and $D(z)$ is the growth factor

of linear density fluctuations normalized such that $(1+z)D(z) \to 1$ during the matter era. (For example, $D(0) = 0.7646$ for $\Omega_M = 0.277$, $\Omega_\Lambda = 0.723$, and $w = -1$.)

Before we show the numerical calculations, we will first try to analytically explore Eq. (22) for the case of a modified initial state, allowing us to estimate the bispectrum shape.

An important observation in what follows is that $W_R(k)$ oscillates rapidly for $k \gtrsim 1/R$, so that the integral of $\mathcal{F}_R(k)$ is dominated by $k_1 \approx 1/R$. Therefore, when we are interested in $k \ll k_1$, the integral of $\mathcal{F}_R(k)$ is dominated by the squeezed configuration, and is approximated as

$$\mathcal{F}_R(k) \approx \frac{1}{4\sigma_R^2 P_\zeta(k)} \int \frac{d^3k_1}{(2\pi)^3} \mathcal{M}_R^2(k_1) B_\zeta(k_1, k_1, k). \quad (28)$$

We can insert the squeezed configuration local bispectrum and calculate

$$\mathcal{F}_R(k) \approx \frac{3}{5} f_{\rm NL}. \quad (29)$$

The second term in the parenthesis in Eq. (22) vanishes for this case and we find $\Delta b(k, R) \propto 1/k^2$ [18–20].

For the bispectrum for a modified initial state, which goes as $1/k_1^2 k^4$, we instead find

$$\mathcal{F}_R(k) \propto \frac{\bar{k}_1(R)}{k}, \quad (30)$$

where

$$\bar{k}_1(R) \equiv \frac{1}{\sigma_R^2} \int \frac{d^3k_1}{(2\pi)^3} k_1 \mathcal{M}_R^2(k_1) P_\zeta(k_1). \quad (31)$$

One may interpret $\bar{k}_1$ as a characteristic wavenumber for the short-wavelength mode in the squeezed configuration. Thus, we expect the modified-state bispectrum to produce a scale-dependent bias which grows faster (by a factor of $\bar{k}_1/k \approx 1/(kR)$) for small values of k than that for the local-form bispectrum.

What about the second term in the brackets in Eq. (22)? If we note that the extra k factor in the integrand of Eq. (31) (as compared with the integrand for σ_R^2) is evaluated at roughly $1/R$, we get $\bar{k}_1(R) \approx 1/R$ and $d\ln\mathcal{F}_R(k)/d\ln R \approx -1$.

On the other hand, σ_R^2 is dominated by the power spectrum of matter density fluctuations at $k \approx 1/R$. Approximating the power spectrum of matter density fluctuations as a power-law near $k \approx 1/R$, i.e., $\mathcal{M}_R^2(k) P_\zeta(k)|_{k\approx R^{-1}} \propto k^{n_{\rm eff}(R)}$, one obtains $d\ln\sigma_R/d\ln R = -[n_{\rm eff}(R)+3]/2$. For example, $n_{\rm eff}(R) = -2.2$, -1.8, and -1.6 for $R = 1$, 5, and 10 h^{-1} Mpc (or $M = 3.2\times10^{11}$, 4.0×10^{13}, and 3.2×10^{14} $h^{-1}\,M_\odot$), respectively.

Therefore, while this second term changes the amplitude of $\Delta b(k, R)$ by a factor of $1 + \frac{2}{[n_{\rm eff}(R)+3]\delta_c(b_1-1)}$, it does not change the k-dependence of $\Delta b(k, R)$. We thus expect the k-dependence of the scale-dependent bias for a modified initial state to be given by $\Delta b(k, R) \propto 1/k^3$. This scaling was also predicted by [36].

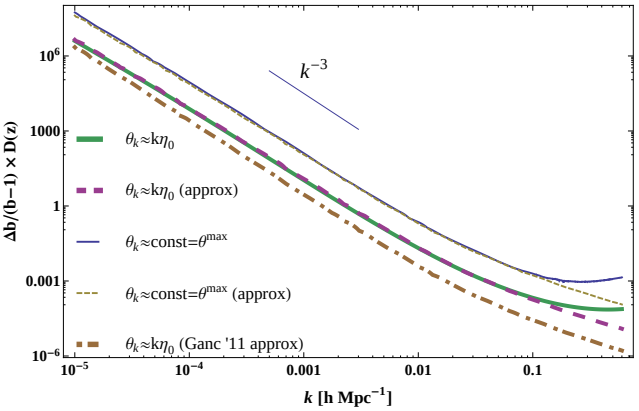

FIG. 1. Scale-dependent halo-bias from single-field inflation with a non-standard initial state, using a smoothing scale of $R = 1\ h^{-1}$ Mpc. The occupation number is $N = 0.5$, the slow-roll parameter $\epsilon = 0.01$, and the initial conformal time $|\eta_0| = 1.0\times10^6$ Mpc (the results are insensitive to the exact choice of η_0, so long as it is large). The bottom three (thicker) lines show the more natural case where $\theta_k \approx k\eta_0$, while the top two (thinner) lines show the case when $\theta_k \approx$ const is chosen to give the maximal halo bias. The dashed lines show the new approximations given by Eqs. (19) and (20), while the dot-dashed line shows the approximation used in [16] (which is equal to Eqs. (19) and (20) without the last lines).

In principle, the second term can change the amplitude of $\Delta b(k, R)$ by a large factor for low-mass halos whose bias is closer to unity [35]. Nevertheless, as we are focused on the shape of $\Delta b(k, R)$ rather than on the amplitude, we will ignore this factor. Then, Eq. (22) simplifies to

$$\begin{aligned}\frac{\Delta b(k,R)}{b_1-1} =& \frac{1}{8\pi^2\sigma_R^2}\frac{\delta_c}{\mathcal{M}_R(k)P_\zeta(k)k}\int_0^\infty {\rm d}k_1\, k_1\mathcal{M}_R(k_1) \\ &\times\int_{|k_1-k|}^{k_1+k}{\rm d}k_2\, k_2\mathcal{M}_R(k_2)B_\zeta(k_1,k_2,k) \\ =& \frac{1}{20\pi^2 D(z)\tilde{\sigma}_R^2}\frac{\delta_c}{\Omega_M H_0^2 k^3 P_\zeta(k)T(k)W_R(k)} \\ &\times\int_0^\infty {\rm d}k_1\, k_1^3 T(k_1)W_R(k_1) \\ &\times\int_{|k_1-k|}^{k_1+k}{\rm d}k_2\, k_2^3 T(k_2)W_R(k_2)B_\zeta(k_1,k_2,k),\end{aligned} \quad (32)$$

which agrees with the formula first derived by [20]. Here, $\tilde{\sigma}_R \equiv \sigma_R/D(z)$, which is independent of z.

To evaluate Eq. (32) we will use $R = 1\ h^{-1}$ Mpc (corresponding to $M = 3.2\times10^{11}\ h^{-1}\,M_\odot$). Also, in order to determine the factor $H^6/\dot{\phi}^2$ which appears in the bispectrum, we use the WMAP 5-year normalization, $k_0^3 P_\zeta(k_0)/(2\pi^2) = 2.41\times10^{-9}$ for $k_0 = 0.002$ Mpc^{-1} [22],

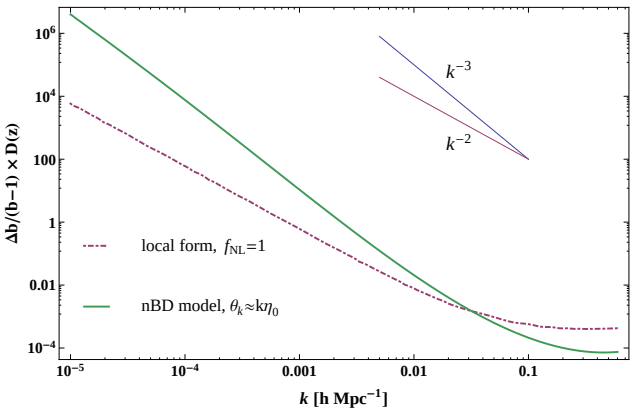

FIG. 2. Scale-dependent bias from the local-form bispectrum (dot-dashed line) versus the modified initial-state case described herein (solid line). The parameters here are the same as in Fig. 1, with $f_{\rm NL} = 1$ for the local-form bispectrum. The difference in scaling between the models is quite evident.

in Eq. (12):

$$\frac{k_0^3 P_\zeta(k_0)}{2\pi^2} = \frac{1}{8\pi^2}\frac{H^2}{\epsilon}\left(1 + 2N + 2\sqrt{N(N+1)}\cos\theta\right), \tag{33}$$

where $\epsilon \equiv (1/2)\dot\phi^2/H^2$ is the slow-roll parameter; for $\theta_k \approx k\eta_0$, the term in parenthesis simply becomes $(1 + 2N)$. This relation gives H^2 for a given ϵ, N, and θ.

We now insert the full bispectrum (Eq. (15)) into Eq. (32) and numerically integrate for the halo bias. Fig. 1 shows the results of the numeric integration for $\epsilon = 0.01$, $N = 0.5$, and θ_k for both scenarios ($\theta_k = k\eta_0$ and $\theta = $ const, with θ chosen to maximize Δb). We do find the expected k^{-3} scaling, which can also be seen by comparison with the local form in Fig. 2.

Fig. 1 also shows the halo bias as calculated from the approximation given in Eq. (19), as well as from the earlier approximation from [16] (which is Eq. (19) without the last line). One sees that the full calculation and the new approximation are very similar except on very small scales (near the smoothing scale); by contrast, the old approximation is off in absolute scale. (There is also a slight change in shape, due to the terms that depend on $k\eta_0$).

VI. μ-TYPE DISTORTION OF THE BLACK-BODY SPECTRUM OF CMB

A. Motivation and background

Diffusion damping of acoustic waves heats CMB photons and creates spectral distortions in the black-body spectrum of the CMB [37]. However, this distortion is erased, maintaing a black-body spectrum for the CMB, as long as photon non-conserving processes are effective. According to [38], double-Compton scattering ($e^- + \gamma \to e^- + 2\gamma$) is an effective thermalization process for $z > z_i \approx 2\times 10^6$. After this epoch, however, this process shuts off and the spectral distortions from diffusion damping cannot be smoothed from the CMB spectrum. Since elastic Compton scattering ($e^- + \gamma \to e^- + \gamma$) continues to be effective until $z_f \approx 5\times 10^4$, the photons can still achieve equilibrium but with a conserved photon number. The result is a Bose-Einstein distribution with a non-zero chemical potential, μ (rescaled by k_BT to be dimensionless), an effect known as the "μ-type distortion" of the black-body spectrum of the CMB, and it affects the distribution by

$$\frac{1}{e^{h\nu/(k_BT)} - 1} \to \frac{1}{e^{h\nu/(k_BT)+\mu} - 1}; \tag{34}$$

a positive μ reduces the number of photons at low frequencies. Finally, after z_f, even elastic Compton scattering is inefficient and photons fall out of kinetic equilibrium with electrons, leaving only the so-called "y-type distortion" [39]. As it would be difficult to distinguish among the y-distortions created by the heating of CMB photons due to diffusion damping, by the cosmic reionization ($z \approx 10$), and by the thermal Sunyaev-Zel'dovich effect [39] from groups and clusters of galaxies ($z \lesssim 3$) [40], we shall focus on the μ-type distortion in this paper.

Diffusion damping occurs near the damping scale given as follows. Over the redshifts of interest, $z \approx 5\times 10^4 - 2\times 10^6$, the expansion rate of the universe is dominated by radiation, $H(z) \propto (1+z)^2$, and the effect of baryon density on the photon-baryon fluid is negligible. Therefore, the damping scale, k_D, is given by [41]

$$k_D^{-2} = \int_0^\eta d\eta' \frac{8}{45\sigma_T n_e a} = -\int_\infty^z dz' \frac{8(1+z)}{45\sigma_T n_e H}, \tag{35}$$

which gives

$$k_D \approx 130\ [(1+z)/10^5]^{3/2}\ {\rm Mpc}^{-1}. \tag{36}$$

Meanwhile, the heat generated by diffusion damping, Q, is given by

$$Q = \frac{1}{4}\rho_\gamma \langle\delta_\gamma^2\rangle, \tag{37}$$

where ρ_γ is the photon energy density and δ_γ is the photon energy density contrast. The coefficient 1/4 merits further explanation. Naively, it would be $c_s^2 = 1/3$, where $c_s = 1/\sqrt{3}$ is the sound speed of the photon fluid. However, a recent computation using second-order perturbation theory [42] reveals that we need an additional factor of 3/4, yielding the number above. This heat is then converted into μ as

$$\mu \approx 1.4\int_{z_f}^\infty dz \frac{1}{\rho_\gamma}\frac{dQ}{dz} e^{-(z/z_i)^{5/2}} \approx \frac{1.4}{4}\left[\langle\delta_\gamma^2\rangle(z_i) - \langle\delta_\gamma^2\rangle(z_f)\right]. \tag{38}$$

The diffusion damping scales at z_i and z_f are given by $k_D(z_i) \approx 12000$ Mpc^{-1} and $k_D(z_f) \approx 46$ Mpc^{-1}, respectively. Therefore, the μ-type distortion is created by the (squared) photon density perturbation on very small scales. This property allows us to probe the power spectrum on such small scales [37, 43].

Pajer and Zaldarriaga recently pointed out that a nonzero bispectrum in the squeezed configuration makes the distribution of μ on the sky *anisotropic*, and that this anisotropy of μ is correlated with the temperature anisotropy of the CMB, which measurements are on scales much larger than the damping scale [21]. This allows us to measure the bispectrum in the squeezed configuration with a larger value of k_1/k than previously thought possible. The smallest possible wavenumber one can measure from the CMB anisotropy in the sky corresponds to the quadrupole, i.e., $k \approx 2/r_L \approx 1.4 \times 10^{-4}$ Mpc^{-1}, where $r_L \approx 14000$ Mpc is the comoving distance to the last scattering surface at $z_L = 1090$. This gives $k_1/k \approx k_D/k = 3.3 \times 10^5 - 8.6 \times 10^7$, which is far greater than that accessible from the temperature anisotropy of the CMB in $l = 2 - 3000$, i.e., $k_1/k = 1 - 1500$, or that accessible from the scale-dependent bias of LSS: $k_1/k \approx 1/(kR) \approx 10^3$ for $k \approx 10^{-3}\ h$ Mpc^{-1} (the lowest wavenumber that can be plausibly measured from the LSS data in near future) and $R \approx 1\ h$ Mpc.

B. Cross-power spectrum of CMB temperature anisotropy and μ-type distortion

First, we decompose the CMB temperature anisotropy on the sky into spherical harmonics: $\delta T(\hat{n})/T = \sum_{lm} a^T_{lm} Y_{lm}(\hat{n})$. The spherical harmonics coefficients are related to the primordial curvature perturbation as

$$a^T_{lm} = \frac{12\pi}{5}(-i)^l \int \frac{d^3k}{(2\pi)^3} \zeta(\mathbf{k}) g_{Tl}(k) Y^*_{lm}(\hat{k}) \,, \qquad (39)$$

where $g_{Tl}(k)$ is the radiation transfer function. Our sign and normalization are such that $g_{Tl}(k) \to -j_l(kr_L)/3$ in the Sachs-Wolfe limit. In other words, $\delta T(\hat{n})/T \to -\zeta(\hat{n}r_L)/5$ in the Sachs-Wolfe limit. However, we will not use the Sachs-Wolfe limit (except for comparison), and instead use $g_{Tl}(k)$ as computed from a linear Boltzmann code [44].

Next, we similarly decompose the distribution of μ measured on the sky, $\mu(\hat{n})$, into spherical harmonics: $\mu(\hat{n}) = \sum_{lm} a^\mu_{lm} Y_{lm}(\hat{n})$. Following [21], we write

$$a^\mu_{lm} = 18\pi(-i)^l \int \frac{d^3k_1 d^3k_2}{(2\pi)^6} Y^*_{lm}(\hat{k}) \zeta(\mathbf{k}_1)\zeta(\mathbf{k}_2) W\left(\frac{k}{k_s}\right) \times \\ \times j_l(kr_L) \langle \cos(k_1 r)\cos(k_2 r)\rangle_p \left[e^{-(k_1^2+k_2^2)/k_D^2(z)}\right]^{z_i}_{z_f} , \qquad (40)$$

with $\mathbf{k}_1 + \mathbf{k}_2 + \mathbf{k} = 0$. (Note that the coefficient of our expression is 18π instead of 24π because of the factor of 3/4, mentioned earlier, from [42]). Here, $W(x) \equiv 3j_1(x)/x$ is a filter function; k_s is the scale over which the damped acoustic waves are averaged to give heat (and which we will take to be equal to $k_D(z_f)$ to obtain a lower bound on the μ-distortion); $r_L \approx 14$ Gpc is the distance to the surface of last scattering; $3\cos(kr)e^{-k^2/k_D^2}$ comes from the small-scale limit of the photon linear transfer function; and $\langle\rangle_p$ denotes an average over the oscillation period.

Correlating Eqs. (39) and (40), we find

$$C_l^{\mu T} = \frac{27}{20\pi^3} \int_0^\infty k_1^2 dk_1 \left[e^{-2k_1^2/k_D^2(z)}\right]^{z_i}_{z_f} \\ \times \int_0^\infty k^2 dk\ W\left(\frac{k}{k_s}\right) B_\zeta(k_1, k_2, k) j_l(kr_L) g_{Tl}(k), \qquad (41)$$

with $k_s \approx k_D(z_f)$.

In order to quantify how well we can measure $C_l^{\mu T}$ in real data, we shall estimate the cumulative signal-to-noise ratio, S/N, from

$$\left(\frac{S}{N}\right)^2 = \sum_l^{l_{\rm max}} (2l+1) \frac{(C_l^{\mu T})^2}{C_l^{TT} C_l^{\mu\mu,N}}. \qquad (42)$$

Here, we have assumed that the temperature data on large scales are dominated by the signal (which is already the case for the WMAP data), while the μ-type distortion data are dominated by noise.

C. Estimating the noise level of μ: absolutely calibrated experiments

One can relate μ to a small change in the CMB photon intensity, $I_\nu = (2h\nu^3/c)(e^{x+\mu} - 1)^{-1}$, as

$$\delta I_\nu = \left.\frac{\partial I_\nu}{\partial \mu}\right|_{\mu=0} \mu = -\frac{2h\nu^3}{c^2} \frac{e^x}{(e^x-1)^2}\mu \\ = -2.70 \times 10^{-18}\ \text{W m}^{-2}\ \text{Hz}^{-1}\ \text{sr}^{-1} \frac{x^3 e^x}{(e^x-1)^2}\mu, \qquad (43)$$

where $x \equiv h\nu/(k_B T) = \nu/(56.80\ \text{GHz})$, for $T = 2.725$ K. This gives

$$\frac{\mu}{10^{-8}} = -\frac{(e^x-1)^2}{x^3 e^x} \frac{\delta I_\nu}{2.70 \times 10^{-26}\ \text{W m}^{-2}\ \text{Hz}^{-1}\ \text{sr}^{-1}}, \qquad (44)$$

which can be used to estimate the noise level of μ from that of I_ν. A factor $\frac{(e^x-1)^2}{x^3 e^x}$ is typically of order unity: $\frac{(e^x-1)^2}{x^3 e^x} = 1.038$, 0.7307, 0.6568, and 0.8804 for $\nu = 60$, 100, 150, and 240 GHz, respectively.

For example, a proposed satellite experiment, PIXIE [45], is designed to have a typical noise level of $\delta I_\nu = 4 \times 10^{-24}$ W m^{-2} Hz^{-1} sr^{-1} within each of 49152 equal-area pixels covering the full sky and each of 400 spectral

channels covering 30 GHz to 6 THz with a 15 GHz bandwidth. Averaging over the full sky, PIXIE would reach $|\mu| \approx 0.5 \times 10^{-8}$ at 100 GHz.

We shall assume that noise is white. The white noise level in the power spectrum can be calculated as:

$$\begin{aligned} C_l^{\mu\mu,N} =& (1\sigma\text{-uncertainty in } \mu \text{ per pixel})^2 \\ & \times (\text{Solid angle of a pixel in units of steradians}) \\ & \times b_l^{-2}, \end{aligned} \tag{45}$$

where b_l is the the so-called beam transfer function, which is the spherical harmonics coefficients of an experimental beam profile. For a Gaussian beam with a full-width-at-half-maximum of θ_b, b_l is given by

$$b_l = \exp\left(-\frac{l^2\theta_b^2}{16\ln 2}\right). \tag{46}$$

For PIXIE, we shall take the 1σ-uncertainty in μ averaged over the full sky to be 10^{-8}. Therefore, the white noise level in the power spectrum is given by $4\pi \times 10^{-16}$ [21]. Their beam has $\theta_b = 1.6^\circ$, yielding $C_l^{\mu\mu,N} = 4\pi \times 10^{-16} \times e^{l^2/84^2}$.

D. Estimating the noise level of μ: relatively calibrated experiments

One must have an absolutely-calibrated experiment such as PIXIE in order to measure a uniform μ. However, an interesting implication of a non-zero bispectrum in the squeezed configuration is that μ becomes anisotropic. This induces a position-dependent temperature fluctuation as $h\nu/(kT) \to h\nu/(kT) + \mu$, i.e.,

$$T \to T(\hat{n}) = \frac{2.725 \text{ K}}{1 + \frac{\mu(\hat{n})}{x}}. \tag{47}$$

The level of anisotropy is thus

$$\frac{\delta T(\hat{n})}{T} \approx -\frac{\delta\mu(\hat{n})}{x}, \tag{48}$$

where $\delta\mu$ is a fluctuating part of μ, i.e., $\mu(\hat{n}) = \bar{\mu} + \delta\mu(\hat{n})$. Therefore, in principle, experiments which are calibrated to the CMB dipole such as WMAP and Planck, as well as the proposed LiteBIRD [46], are also capable of measuring this effect by making a map of $\delta\mu(\hat{n})$ from the difference between temperature maps at two different frequencies, ν_1 and ν_2. Then, the formula for the noise power spectrum becomes

$$\begin{aligned} C_l^{\mu\mu,N} =& \left[\frac{\nu_1\nu_2/(\nu_1-\nu_2)}{56.80 \text{ GHz}}\right]^2 \\ & \times [(1\sigma\text{-uncertainty in } \delta T/T \text{ per pixel at } \nu_1)^2 \\ & + (1\sigma\text{-uncertainty in } \delta T/T \text{ per pixel at } \nu_2)^2] \\ & \times (\text{Solid angle of a pixel in units of steradians}) \\ & \times b_l^{-2}. \end{aligned} \tag{49}$$

According to the Planck Blue Book [47], the expected sensitivities of Planck at 100 and 143 GHz are $\delta T/T = 2.5 \times 10^{-6}$ per $10' \times 10'$ pixel, and $\delta T/T = 2.2 \times 10^{-6}$ per $7.1' \times 7.1'$ pixel, respectively. The in-flight performance then shows that the achieved noise level is 70% of the expectation, and the beam sizes at 100 and 143 GHz are $9.4'$ and $7.2'$, respectively [48]; thus, we estimate Planck's sensitivity to $\delta\mu$ measured from maps at 100 and 143 GHz as $C_l^{\mu\mu,N} \approx 1.1 \times 10^{-15} \times e^{l^2/861^2}$. This is comparable to the above estimate for PIXIE, which is based on the *absolute* measurement of the CMB spectrum.

However, as the sensitivity of PIXIE (and LiteBIRD) to CMB anisotropy is at least an order of magnitude better than that of Planck, if we focus only on the spatially-varying part of μ rather than the uniform part of μ, then it may be possible to increase the sensitivity to $C_l^{\mu T}$. The expected noise power spectrum is of order $C_l^{\mu\mu,N} \approx 10^{-17}$ or better, according to Eq. (49). In other words, the signal-to-noise of $C_l^{\mu T}$ can be improved by an order of magnitude as compared to the case where we look at absolute measurements of μ.

In order to do this in practice, we must calibrate instruments at different frequencies so that they have the equal response to the thermal CMB. To estimate the required precision for calibration, let us suppose that the response of one instrument at ν_1 is different from that of another at ν_2 by ϵ. Then, the difference between two maps at these frequencies will yield $(\delta T/T)(\nu_1) - (\delta T/T)(\nu_2) = \epsilon(\delta T/T)$, where δT is the CMB anisotropy. This residual will be confused as a signal in $\delta\mu$, such that $\delta\mu = \left[\frac{\nu_1\nu_2/(\nu_1-\nu_2)}{56.80 \text{ GHz}}\right]\epsilon(\delta T/T)$ which, in turn, will give a contamination of $C_l^{\mu T}$ given by

$$\begin{aligned} & \frac{l(l+1)C_{l,\text{contamination}}^{\mu T}}{2\pi} \\ & = 2 \times 10^{-10}\epsilon\left[\frac{\nu_1\nu_2/(\nu_1-\nu_2)}{56.80 \text{ GHz}}\right]\left[\frac{l(l+1)C_l^{TT}/2\pi}{2 \times 10^{-10}}\right]. \end{aligned} \tag{50}$$

As we shall show below (also see [21]), $C_l^{\mu T}$ from the local-form bispectrum is of order $l(l+1)|C_l^{\mu T}|/(2\pi) \approx 4 \times 10^{-17} f_{\rm NL}$. Therefore, the required precision for the calibration is given by

$$\left[\frac{\nu_1\nu_2/(\nu_1-\nu_2)}{56.80 \text{ GHz}}\right]\epsilon \ll 2 \times 10^{-7} f_{\rm NL}. \tag{51}$$

For example, the calibration precision of the WMAP data is $\epsilon = 2 \times 10^{-3}$ [49], and thus the contamination of $C_l^{\mu T}$ due to the calibration mismatch is negligible for $f_{\rm NL} \gg 10^4\left[\frac{\nu_1\nu_2/(\nu_1-\nu_2)}{56.80 \text{ GHz}}\right]$. To search for a $C_l^{\mu T}$ signal, future CMB experiments such as LiteBIRD may wish to place more emphasis on the relative calibration of their instruments. Note that the signal from a modified initial state will be much larger, $l(l+1)|C_l^{\mu T}|/(2\pi) \approx \frac{2\times 10^{-11}}{l}(\frac{\dot{\phi}^2}{2H^2}/0.01)$ (see Section VI F), so the required precision for the calibration can be relaxed greatly.

Another factor which may limit the utility of relatively calibrated instruments is foreground contamination. In principle, foreground contamination can be removed by using multi-frequency data, since the frequency spectrum of the foreground (roughly proportional to ν^{-3}, ν^{-2}, and ν^2 for synchrotron, free-free, and dust emission, respectively) is different from that of μ-type distortion ($\propto \nu^{-1}$). Detailed study of foreground contamination is beyond the scope of this paper, but it is worth studying this in detail once the required calibration precision is reached.

E. Results for the local-form bispectrum

Before we discuss $C_l^{\mu T}$ from the modified initial state effect, let us discuss $C_l^{\mu T}$ from the local-form bispectrum. Using the local-form bispectrum (Eq. (3)) in the expression for $C_l^{\mu T}$ (Eq. (41)), we find

$$C_l^{\mu T} = \frac{81}{25\pi^3} f_{\rm NL} \int_0^\infty k_1^2 dk_1 \left[e^{-2k_1^2/k_D^2(z)}\right]_{z_f}^{z_i} P_\zeta(k_1) \times \int_0^\infty k^2 dk\ W\left[\frac{k}{k_D(z_f)}\right] P_\zeta(k) j_l(kr_L) g_{Tl}(k). \quad (52)$$

For a scale-invariant spectrum, $P_\zeta = \frac{2\pi^2}{k^3}\Delta_\zeta^2$ with $\Delta_\zeta^2 = 2.4\times10^{-9}$, we find

$$C_l^{\mu T} = \frac{324\pi}{25} f_{\rm NL} \Delta_\zeta^4 \ln\left[\frac{k_D(z_i)}{k_D(z_f)}\right] \times \int_0^\infty \frac{dk}{k}\ W\left[\frac{k}{k_D(z_f)}\right] j_l(kr_L) g_{Tl}(k). \quad (53)$$

While we use the exact radiation transfer function calculated from the linear Boltzmann code (except as indicated), it is instructive to obtain an analytical expression for the Sachs-Wolfe limit, $g_{Tl}(k) \to -j_l(kr_L)/3$. As the wavenumbers that are responsible for the Sachs-Wolfe regime are much smaller than $k_D(z_f)$, one can approximate $W\left[\frac{k}{k_D(z_f)}\right] \to 1$. We then find

$$C_l^{\mu T} \to -\frac{54\pi}{25} f_{\rm NL} \Delta_\zeta^4 \ln\left[\frac{k_D(z_i)}{k_D(z_f)}\right] \frac{1}{l(l+1)} \approx -3.5\times10^{-17} f_{\rm NL} \times \frac{2\pi}{l(l+1)}. \quad (54)$$

This result agrees with that obtained by [21] up to a factor of 3/4 recently found by [42]. Therefore, on large scales where the Sachs-Wolfe approximation is valid, the cross-power spectrum is "scale invariant," in a sense that $l(l+1)C_l^{\mu T}$ =constant. The overall sign is negative for a positive $f_{\rm NL}$ because, for a positive curvature perturbation ζ, $\delta T/T = -\zeta/5$ is negative whereas the fluctuation in $\delta\mu \propto f_{\rm NL}\zeta$ is positive for a positive $f_{\rm NL}$.

How good is the Sachs-Wolfe approximation? In Figure 3, we compare the Sachs-Wolfe approximation with the exact calculation. We find that the Sachs-Wolfe approximation breaks down at $l \approx 10$, and the acoustic oscillation changes the sign of $C_l^{\mu T}$ at $l \approx 40$. As $C_l^{\mu T}$ crosses zero at $l \approx 40$, we expect the signal-to-noise ratio to grow more slowly with increasing multipole than with the Sachs-Wolfe approximation.

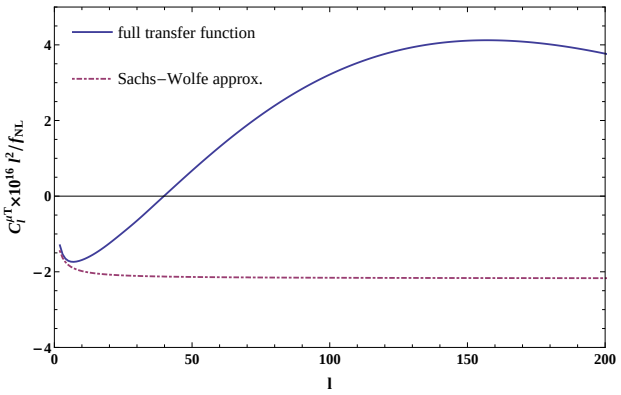

FIG. 3. $C_l^{\mu T}$, the cross-power spectrum of the μ-type distortion and the CMB temperature anisotropy, from the local-form bispectrum with $f_{\rm NL} = 1$. The solid line shows $C_l^{\mu T}$ using the full radiation transfer function, while the dot-dashed line shows it using the Sachs-Wolfe approximation. The amplitude of $C_l^{\mu T}$ is linearly proportional to $f_{\rm NL}$.

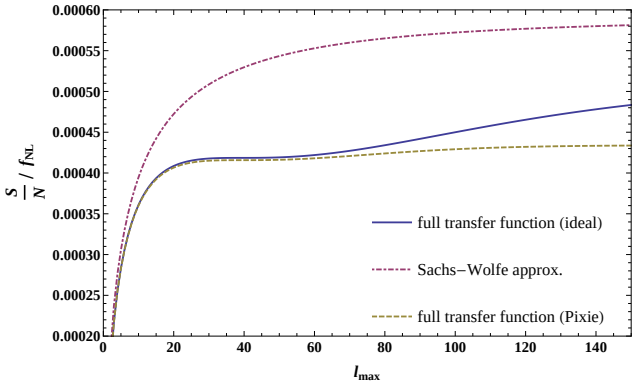

FIG. 4. Signal-to-noise ratio of $C_l^{\mu T}$ from the local-form bispectrum with $f_{\rm NL} = 1$. The bottom two lines show $C_l^{\mu T}$ using the full radiation transfer function, while the dot-dashed line shows it using the Sachs-Wolfe approximation. The solid, dashed line is for $\theta_b = 0$ (ideal) and 1.6° (PIXIE), respectively. The noise level is $C_l^{\mu\mu,N} = 4\pi\times10^{-16} e^{l^2\theta_b^2/(8\ln 2)}$ for all cases (i.e., the r.m.s. uncertainty of μ averaged over the full sky is 10^{-8}). The signal-to-noise is proportional to $f_{\rm NL}$ and is inversely proportional to the r.m.s. uncertainty of μ.

In Figure 4, we show the cumulative signal-to-noise ratio of $C_l^{\mu T}$ from the local-form bispectrum as a function of the maximum multipole, $l_{\rm max}$. We find that the Sachs-Wolfe approximation overestimates the signal-to-noise ratio by about 40%. Due to the sign change in $C_l^{\mu T}$, the signal-to-noise ratio does not grow between $l_{\rm max} \approx 20$ and 80.

For PIXIE's specification with $\theta_b = 1.6°$ and $C_l^{\mu\mu,N}$ =

$4\pi \times 10^{-16}$, the signal-to-noise ratio reaches $S/N = 4.3 \times 10^{-4} f_{\rm NL}$. Therefore, PIXIE would be able to see the signal if $f_{\rm NL} \gg 2300$. If PIXIE's detectors can be calibrated so that the difference between maps at different frequencies cancels the CMB anisotropy to the required precision, then S/N can improve by an order of magnitude. Reducing the beam size would not help much because the signal-to-noise ratio grows only logarithmically with $l_{\rm max}$ [21].

F. Results for the modified initial state bispectrum

We now calculate $C_l^{\mu T}$ from the modified initial state bispectrum. We start from

$$\begin{aligned} C_l^{\mu T} =& \frac{27}{20\pi^3}\frac{H^6}{\dot\phi^2}\xi(N)\int_0^\infty dk_1 \left[e^{-2k_1^2/k_D^2(z)}\right]_{z_f}^{z_i} \\ & \times \int_0^\infty \frac{dk}{k^2}\, W\left[\frac{k}{k_D(z_f)}\right] j_l(kr_L) g_{Tl}(k)\kappa(k\eta_0) \\ =& \frac{27}{40\sqrt{2}\pi^{5/2}}\frac{H^6}{\dot\phi^2}\xi(N)[k_D(z_i)-k_D(z_f)] \\ & \times \int_0^\infty \frac{dk}{k^2}\, W\left[\frac{k}{k_D(z_f)}\right] j_l(kr_L) g_{Tl}(k)\kappa(k\eta_0), \end{aligned} \tag{55}$$

where $\xi(N)$ is given by the second lines of Eqs. (19) and (20) and $\kappa(k\eta_0)$ is given by the last lines of Eqs. (19) and (20). Once again, a factor $H^6/\dot\phi^2$ will be calculated from the normalization of $P_\zeta(k)$ for a given ϵ, N, and θ (see Eq. (33)).

To obtain an order-of-magnitude estimation, let us set $\kappa = 1$ and take the Sachs-Wolfe limit. We then obtain

$$\begin{aligned} C_l^{\mu T} \to & -\frac{9}{40\sqrt{2}\pi^{5/2}}\frac{H^6}{\dot\phi^2}\xi(N)[k_D(z_i)-k_D(z_f)] \\ & \times \int_0^\infty \frac{dk}{k^2}\, j_l^2(kr_L) \\ =& -\frac{9}{320\sqrt{2}\pi^{3/2}}\frac{H^6}{\dot\phi^2}\frac{\xi(N)[k_D(z_i)-k_D(z_f)]r_L}{\left(l+\frac{3}{2}\right)\left(l+\frac{1}{2}\right)\left(l-\frac{1}{2}\right)}. \end{aligned} \tag{56}$$

Therefore, $C_l^{\mu T}$ from the modified initial state falls as $C_l^{\mu T} \propto l^{-3}$, which is faster than that from the local form, $\propto l^{-2}$. However, the amplitude is proportional to $k_D(z_i) r_L \approx 1.7 \times 10^8$ instead of $\ln[k_D(z_i)/k_D(z_f)] \approx 5.5$, which leads to a large amplification of the signal relative to the local form.

In Figure 5, we compare the shapes of $C_l^{\mu T}$ from the local-form bispectrum (solid line) and from the modified initial state bispectrum (dot-dashed line). As expected, for the low multipoles $l \lesssim 40$ (where $C_l^{\mu T}$ is negative), $C_l^{\mu T}$ from the modified initial state is steeper (by a factor of $1/l$) than that from the local form, whereas for high multipoles $l \gtrsim 40$ (where $C_l^{\mu T}$ is positive), $C_l^{\mu T}$ from the modified initial state is shallower (because it diminishes faster by $1/l$).

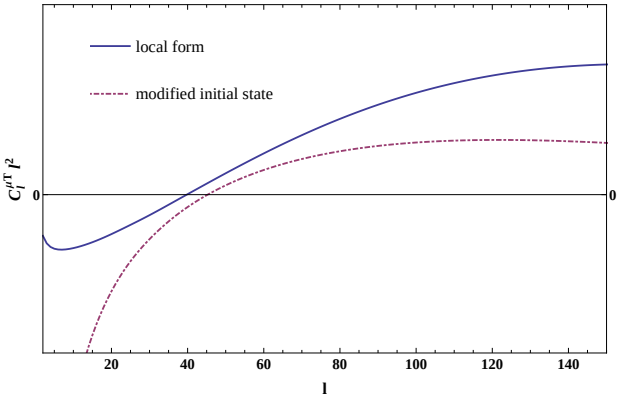

FIG. 5. A comparison of the shapes of $C_l^{\mu T}$ (the cross-power spectra of the μ-type distortion and the CMB temperature anisotropy) from the local-form bispectrum (solid line) and the modified state bispectrum (dot-dashed line). The amplitudes of the graphs are scaled so they can both appear in the same figure; therefore, the overall amplitude is arbitrary.

In order to better compare the modified initial state result (Eq. (56)) with the local-form result (Eq. (54)), let us use the power spectrum normalization, $\Delta_\zeta^2 = H^2(1+2N)/(8\pi^2\epsilon)$ (Eq. (33)), to rewrite Eq. (56) as

$$\begin{aligned} C_l^{\mu T} &= -\frac{9\pi^{5/2}}{10\sqrt{2}}\Delta_\zeta^4\epsilon\frac{\xi(N)}{(1+2N)^2}\frac{[k_D(z_i)-k_D(z_f)]r_L}{\left(l+\frac{3}{2}\right)\left(l+\frac{1}{2}\right)\left(l-\frac{1}{2}\right)} \\ &\approx \frac{-1.7\times10^{-11}}{l+\frac{3}{2}}\frac{\epsilon}{10^{-2}}\frac{\xi(N)}{(1+2N)^2}\times\frac{2\pi}{l^2-\frac{1}{4}}. \end{aligned} \tag{57}$$

We find the ratio

$$\frac{C_l^{\mu T,\rm nBD}}{C_l^{\mu T,\rm local}} \approx \frac{4.9\times10^5}{(l+\frac{3}{2})f_{\rm NL}}\frac{\epsilon}{10^{-2}}\frac{\xi(N)}{(1+2N)^2}\frac{l(l+1)}{l^2-\frac{1}{4}}. \tag{58}$$

For single-field slow-roll inflation, $f_{\rm NL} \approx \epsilon \approx 10^{-2}$. Therefore, the ratio (Eq. (58)) is $\approx 5\times10^7/l$.

We can verify this ratio in a different way. Heuristically, for a modified initial state, the enhancement of the bispectrum in the squeezed configuration by a factor of $k_1/k \gg 1$ becomes a enhancement of $C_l^{\mu T}$ by a factor of $k_D(z_i) r_L/l = k_D(z_i)/k_{{\rm CMB},l} \approx 2\times10^8/l$, i.e., the ratio of the acoustic damping wavenumber to the wavenumber generating the multipole l, giving close to the ratio above. Note that the biggest contribution to the signal will come from small multipoles (in particular the quadrupole $l = 2$), so the signal boost relative to the local form is indeed large.

In Figure 6, we show the signal-to-noise ratio of $C_l^{\mu T}$ for a modified initial state as a function of the occupation number N. For PIXIE's specification with $\theta_b = 1.6^\circ$ and $C_l^{\mu\mu,N} = 4\pi\times10^{-16} e^{l^2\theta_b^2/(8\ln 2)}$, we find a large signal-to-noise ratio: when the occupation number is $N \approx 0.5$, the signal-to-noise ratios are $S/N \approx 60(\epsilon/10^{-2})$ and $500(\epsilon/10^{-2})$ for $\theta_k \approx k\eta_0$ and $\theta_k \approx$ const, respectively. (Recall that, for the latter case, we have chosen a constant θ_k so that it maximizes the signal.) This large

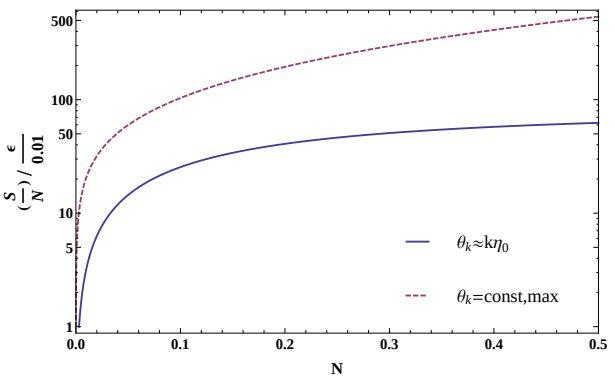

FIG. 6. Signal-to-noise ratio of $C_l^{\mu T}$ from the modified initial state for $\epsilon = 10^{-2}$, as a function of the occupation number N. The top and bottom lines are for $\theta_k \approx$ const (dashed) and $\theta_k \approx k\eta_0$ (solid), respectively. The noise level is $C_l^{\mu\mu,N} = 4\pi \times 10^{-16} e^{l^2/84^2}$ for both cases (i.e., the r.m.s. uncertainty of μ averaged over the full sky is 10^{-8}, and the beam size is 1.6°). The signal-to-noise ratio is proportional to ϵ and is inversely proportional to the r.m.s. uncertainty of μ.

increase in the signal-to-noise ratio relative to the local-form bispectrum is consistent with the analytical estimate given in Eq. (58).

Note that these calculations were done assuming η_0 was finite, i.e., we included the last lines of Eqs. (19) and (20). If we ignore the exponential terms in Eq. (15) by taking $\eta_0 \to \eta_0 + i\epsilon|\eta_0|$ for large $|\eta_0|$, then the signal-to-noise ratio goes down to about ten for $\theta_k \approx k\eta_0$ and $N \approx 0.5$, which is still large enough for detection. Therefore, we should be able to detect $C_l^{\mu T}$ in the PIXIE experiment unless N were very small.

If the calibration of detectors at different frequencies meets the requirements (see Section VI D), then PIXIE would be able to improve its signal-to-noise ratio for detecting $C_l^{\mu T}$ by an order of magnitude. Moreover, if Planck's calibration meets the requirement, Planck would be able to detect this signal. This merits further study.

However, one caveat should be mentioned, namely that these results assume that the cut-off wavenumber, $k_{\rm cut}$, lies above the scales involved in the μ-distortion. If $k_{\rm cut}$ lay within the μ-distortion scales, this model could produce a measurable CMB and LSS signal but have a smaller-than-expected $C_l^{\mu T}$.

VII. CONCLUSION

We have investigated phenomenological consequences of a modification of the initial state of quantum fluctuations generated during single-field slow-roll inflation. In our model, the initial state is given by a Bogoliubov transformation on the standard Bunch-Davies initial vacuum state. A distinctive feature of this model is that the bispectrum of ζ in the squeezed configuration – where one of the wavenumbers, k, is much smaller than the other two, i.e., $k \ll k_1 \approx k_2$ – is enhanced by a factor of k_1/k relative to the local-form bispectrum [15]. This enhancement generates notable effects on the scale-dependent bias of LSS and on the μ-type distortion of the black-body spectrum of CMB.

For LSS, the scale-dependent bias goes as $\bar{k}_1/k^3$ instead of $1/k^2$, where $\bar{k}_1$ is a characteristic wavenumber corresponding to the short-wavelength mode in LSS for a given halo mass (Eq. (31)).

For the μ-type distortion, the squeezed configuration bispectrum can make μ *anisotropic*, which can be measured by cross-correlating a map of μ with a map of CMB temperature anisotropy on large scales [21]. The modified initial state enhances power spectrum $C_l^{\mu T}$ of this cross-correlation by a factor of $k_D r_L$, which corrresponds to the ratio of the wavenumber of the acoustic damping scale to the wavenumber measured by CMB temperature anisotropy on large scales. We predict that an absolutely-calibrated experiment such as PIXIE can detect $C_l^{\mu T}$ unless the occupation number is much smaller than of order unity.

As this effect makes μ anisotropic, one may not even need an absolutely-calibrated experiment. If detectors at different frequencies are calibrated to have the same response to thermal CMB with the sufficient precision, then relatively-calibrated experiments such as Planck and LiteBIRD could detect this signal.

We acknowledge that our derivation of the bispectrum from a modified initial state is limited by uncertainties about how to set initial conditions and how to translate these conditions into a proper calculational framework. While we think that the calculations presented in this paper capture plausible outcomes of a modified initial state, more investigation on quantum field theory with such a state is still necessary. That this model predicts such interesting signatures in LSS and the CMB motivates further study.

Finally, while we have focused only on the bispectrum in the squeezed configuration in this paper, this model also predicts a large bispectrum in the folded limit, where the largest wavenumber is equal to the sum of the other two wavenumbers, $k_1 = k_2 + k$ [26, 27, 31]. The observational signatures that we have discussed in this paper should come also with the signal in the folded limit, which provides a powerful cross-check of the nature of the detected signal.

ACKNOWLEDGMENTS

Note that a similar analysis on the effect of a modified initial state on the scale-dependent bias is presented in [50].

We would like to thank Xingang Chen, Daan Meerburg, and Enrico Pajer for helpful discussions. This work is supported in part by NSF grant PHY-0758153.

[1] N. Bartolo, E. Komatsu, S. Matarrese, and A. Riotto, Phys. Rept. **402**, 103 (2004), astro-ph/0406398.

[2] E. Komatsu *et al.*, in *astro2010: The Astronomy and Astrophysics Decadal Survey*, Astronomy, Vol. 2010 (2009) p. 158, arXiv:0902.4759 [astro-ph.CO].

[3] X. Chen, Adv.Astron. **2010**, 638979 (2010), arXiv:1002.1416 [astro-ph.CO].

[4] S. Weinberg, Phys.Rev. **D67**, 123504 (2003), arXiv:astro-ph/0302326 [astro-ph].

[5] E. Komatsu *et al.* (WMAP Collaboration), Astrophys.J.Suppl. **192**, 18 (2011), arXiv:1001.4538 [astro-ph.CO].

[6] J. Dunkley *et al.* (ACT Collaboration), Astrophys.J. **739**, 52 (2011), arXiv:1009.0866 [astro-ph.CO]; R. Keisler *et al.* (SPT Collaboration), *ibid.* **743**, 28 (2011), arXiv:1105.3182 [astro-ph.CO].

[7] A. Gangui, F. Lucchin, S. Matarrese, and S. Mollerach, Astrophys.J. **430**, 447 (1994); L. Verde, L. Wang, A. F. Heavens, and M. Kamionkowski, Mon.Not.R.Astron.Soc. **313**, 141 (2000), arXiv:astro-ph/9906301.

[8] E. Komatsu and D. N. Spergel, Phys. Rev. **D63**, 063002 (2001), arXiv:astro-ph/0005036.

[9] J. M. Maldacena, JHEP **05**, 013 (2003), arXiv:astro-ph/0210603.

[10] V. Acquaviva, N. Bartolo, S. Matarrese, and A. Riotto, Nucl.Phys. **B667**, 119 (2003), arXiv:astro-ph/0209156 [astro-ph].

[11] P. Creminelli and M. Zaldarriaga, JCAP **0410**, 006 (2004), arXiv:astro-ph/0407059.

[12] P. Creminelli, G. D'Amico, M. Musso, and J. Norena, JCAP **1111**, 038 (2011), arXiv:1106.1462 [astro-ph.CO].

[13] D. M. Goldberg and D. N. Spergel, Phys.Rev. **D59**, 103002 (1999), arXiv:astro-ph/9811251 [astro-ph]; L. Verde and D. N. Spergel, *ibid.* **D65**, 043007 (2002), arXiv:astro-ph/0108179 [astro-ph]; K. M. Smith and M. Zaldarriaga, Mon.Not.Roy.Astron.Soc. **417**, 2 (2011), arXiv:astro-ph/0612571 [astro-ph]; P. Serra and A. Cooray, Phys.Rev. **D77**, 107305 (2008), arXiv:0801.3276 [astro-ph]; D. Hanson, K. M. Smith, A. Challinor, and M. Liguori, *ibid.* **D80**, 083004 (2009), arXiv:0905.4732 [astro-ph.CO]; V. Junk and E. Komatsu, (2012), arXiv:1204.3789 [astro-ph.CO].

[14] D. Nitta, E. Komatsu, N. Bartolo, S. Matarrese, and A. Riotto, JCAP **0905**, 014 (2009), arXiv:0903.0894 [astro-ph.CO]; P. Creminelli, C. Pitrou, and F. Vernizzi, *ibid.* **1111**, 025 (2011), arXiv:1109.1822 [astro-ph.CO]; N. Bartolo, S. Matarrese, and A. Riotto, *ibid.* **1202**, 017 (2012), arXiv:1109.2043 [astro-ph.CO].

[15] I. Agullo and L. Parker, Phys.Rev. **D83**, 063526 (2011), arXiv:1010.5766 [astro-ph.CO].

[16] J. Ganc, Phys.Rev. **D84**, 063514 (2011), arXiv:1104.0244 [astro-ph.CO].

[17] E. Komatsu, B. D. Wandelt, D. N. Spergel, A. J. Banday, and K. M. Gorski, Astrophys.J. **566**, 19 (2002), arXiv:astro-ph/0107605 [astro-ph]; E. Komatsu *et al.* (WMAP Collaboration), Astrophys.J.Suppl. **148**, 119 (2003), arXiv:astro-ph/0302223 [astro-ph].

[18] N. Dalal, O. Dore, D. Huterer, and A. Shirokov, Phys.Rev. **D77**, 123514 (2008), arXiv:0710.4560 [astro-ph].

[19] A. Slosar, C. Hirata, U. Seljak, S. Ho, and N. Padmanabhan, JCAP **0808**, 031 (2008), arXiv:0805.3580 [astro-ph].

[20] S. Matarrese and L. Verde, Astrophys.J. **677**, L77 (2008), arXiv:0801.4826 [astro-ph].

[21] E. Pajer and M. Zaldarriaga, (2012), arXiv:1201.5375 [astro-ph.CO].

[22] E. Komatsu *et al.* (WMAP Collaboration), Astrophys.J.Suppl. **180**, 330 (2009), arXiv:0803.0547 [astro-ph].

[23] S. Kundu, JCAP **1202**, 005 (2012), arXiv:1110.4688 [astro-ph.CO].

[24] P. R. Anderson, C. Molina-París, and E. Mottola, Phys.Rev. **72**, 043515 (2005), arXiv:hep-th/0504134.

[25] D. Boyanovsky, H. J. de Vega, and N. G. Sanchez, Phys. Rev. D **74**, 123006 (2006), arXiv:astro-ph/0607508.

[26] R. Holman and A. J. Tolley, JCAP **0805**, 001 (2008), arXiv:0710.1302 [hep-th].

[27] P. D. Meerburg, J. P. van der Schaar, and P. S. Corasaniti, JCAP **0905**, 018 (2009), arXiv:0901.4044 [hep-th].

[28] P. Meerburg, J. P. van der Schaar, and M. G. Jackson, JCAP **1002**, 001 (2010), arXiv:0910.4986 [hep-th]; A. Ashoorioon and G. Shiu, *ibid.* **1103**, 025 (2011), arXiv:1012.3392 [astro-ph.CO].

[29] K. Schalm, G. Shiu, and J. P. van der Schaar, JHEP **0404**, 076 (2004), arXiv:hep-th/0401164 [hep-th]; B. Greene, K. Schalm, J. P. van der Schaar, and G. Shiu, in *22nd Texas Symposium on Relativistic Astrophysics*, edited by P. Chen, E. Bloom, G. Madejski, & V. Patrosian (2005) pp. 1–8, arXiv:astro-ph/0503458.

[30] R. Easther, W. H. Kinney, and H. Peiris, JCAP **8**, 1 (2005), arXiv:astro-ph/0505426.

[31] X. Chen, M.-x. Huang, S. Kachru, and G. Shiu, JCAP **0701**, 002 (2007), arXiv:hep-th/0605045 [hep-th].

[32] E. Sefusatti and E. Komatsu, Phys.Rev. **D76**, 083004 (2007), arXiv:0705.0343 [astro-ph].

[33] B. Grinstein and M. B. Wise, Astrophys.J. **310**, 19 (1986); S. Matarrese, F. Lucchin, and S. A. Bonometto, *ibid.* **310**, L21 (1986).

[34] N. Kaiser, Astrophys.J. **284**, L9 (1984).

[35] V. Desjacques, D. Jeong, and F. Schmidt, Phys.Rev. **D84**, 063512 (2011), arXiv:1105.3628 [astro-ph.CO]; **D84**, 061301 (2011), arXiv:1105.3476 [astro-ph.CO].

[36] D. Chialva, ArXiv e-prints (2011), arXiv:1108.4203 [astro-ph.CO].

[37] R. Sunyaev and Y. Zeldovich, Astrophys.Space Sci. **7**, 20 (1970); R. A. Sunyaev and Y. B. Zeldovich, **9**, 368 (1970); R. A. Daly, Astrophys.J. **371**, 14 (1991).

[38] W. Hu and J. Silk, Phys.Rev. **D48**, 485 (1993).

[39] Y. B. Zeldovich and R. A. Sunyaev, Astrophys.Space.Sci. **4**, 301 (1969); R. Sunyaev and Y. Zeldovich, Comments Astrophys. Space Phys. **4**, 173 (1972).

[40] A. Refregier, E. Komatsu, D. N. Spergel, and U.-L. Pen, Phys.Rev. **D61**, 123001 (2000), arXiv:astro-ph/9912180 [astro-ph].

[41] J. Silk, Astrophys.J. **151**, 459 (1968); N. Kaiser, Mon.Not.R.Astron.Soc. **202**, 1169 (1983); S. Weinberg, *Cosmology* (Oxford University Press, Oxford, UK, 2008).

[42] J. Chluba, R. Khatri, and R. A. Sunyaev, (2012), arXiv:1202.0057 [astro-ph.CO].

[43] W. Hu, D. Scott, and J. Silk, Astrophys.J. **430**, L5 (1994), arXiv:astro-ph/9402045 [astro-ph]; J. Chluba

and R. Sunyaev, (2011), arXiv:1109.6552 [astro-ph.CO]; R. Khatri, R. A. Sunyaev, and J. Chluba, Astron.Astrophys. **540**, A124 (2012), arXiv:1110.0475 [astro-ph.CO]; J. Chluba, A. L. Erickcek, and I. Ben-Dayan, (2012), arXiv:1203.2681 [astro-ph.CO].

[44] A code for calculating the radiation transfer function is available at http://www.mpa-garching.mpg.de/~komatsu/CRL/. This code is based on CMBFAST [51].

[45] A. Kogut, D. Fixsen, D. Chuss, J. Dotson, E. Dwek, *et al.*, JCAP **1107**, 025 (2011), arXiv:1105.2044 [astro-ph.CO].

[46] http://cmbpol.kek.jp/litebird/.

[47] The Planck Collaboration, ArXiv Astrophysics e-prints (2006), arXiv:astro-ph/0604069.

[48] P. Ade *et al.* (Planck HFI Core Team), (2011), arXiv:1101.2039 [astro-ph.IM].

[49] G. Hinshaw *et al.* (WMAP Collaboration), Astrophys.J.Suppl. **180**, 225 (2009), arXiv:0803.0732 [astro-ph]; N. Jarosik *et al.*, **192**, 14 (2011), arXiv:1001.4744 [astro-ph.CO].

[50] I. Agullo and S. Shandera, (2012), arXiv:1204.4409 [astro-ph.CO].

[51] U. Seljak and M. Zaldarriaga, Astrophys.J. **469**, 437 (1996), arXiv:astro-ph/9603033 [astro-ph].